RSC Advances

PAPER

View Article Online
View Journal | View Issue

Cite this: *RSC Adv.*, 2021, **11**, 38528

Photocatalysis of nanocomposite titania–natural silica as antibacterial against *Staphylococcus aureus* and *Pseudomonas aeruginosa*†

Annisa Luthfiah,[a] Muhamad Diki Permana,[a] Yusi Deawati,[a] M. Lutfi Firdaus,[b] Iman Rahayu[a] and Diana Rakhmawaty Eddy *[a]

Received 20th September 2021
Accepted 13th November 2021

DOI: 10.1039/d1ra07043f

rsc.li/rsc-advances

The entries of pathogenic bacteria into the human body remain a severe problem to health that can be prevented using antibacterial agents. Meanwhile, the photocatalytic technique using semiconductor nanocomposite TiO_2–SiO_2 has great potential as an antibacterial method. In order to utilize natural resources, SiO_2 supporting materials are obtained from the extraction of beach sand due to the high silica content. Therefore, this study aims to synthesize a nanocomposite of TiO_2 with SiO_2 extracted from beach sand as an antibacterial agent against *Staphylococcus aureus* and *Pseudomonas aeruginosa*. The antibacterial activity test used the dilution and optical density method. Based on XRD analysis, the crystals of TiO_2 in the synthesized composites showed a more dominant anatase structure. Furthermore, Ti–O–Si bonds were identified from the IR spectrum, which showed the interaction between TiO_2 and SiO_2. In addition, SEM-EDX results showed agglomerated spherical particles with a TiO_2–SiO_2 nanocomposite particle size of 40–107 nm. The best antibacterial activity was demonstrated by the 1 : 0.5 TiO_2–SiO_2 nanocomposite, with inactivation percentages of *S. aureus* and *P. aeruginosa* of 98.69% and 97.44%, respectively.

Introduction

Pathogenic bacteria remain a considerable problem for human health,[1] due to the large population and extremely small size, and being located in various environments.[2] These bacteria are capable of infecting humans and causing various diseases such as pleuropneumonia,[3] pneumonia,[4] septicemia,[5] edema,[6] and other dangerous diseases.[2] As a preventative measure, antibacterial agents minimize the harmful effects by inhibiting bacterial growth. In general, these agents consist of organic compounds used as disinfection systems and antibiotics.[7] However, there are certain limitations, such as relatively high toxicity, instability of physical properties to pressure and temperature, and the existence of various antibiotic-resistant strains.[8–10] Consequently, the development of renewable antibacterial agents remains one of the biggest health challenges in the world.[9] Therefore, the interest in safer inorganic disinfectants is increasing.

The use of disinfectants with inorganic substances is usually carried out through photocatalysis, a combination of chemical reactions that require light and photocatalysts to accelerate chemical transformations.[11] Meanwhile, sunlight is the most abundant, clean, and safest sustainable energy source.[12] This process produces radical oxygen species (ROS) capable of inactivating bacteria.[13,14] Furthermore, the efficiency of a photocatalyst is influenced by the surface area of the active reacting sites.[15] Therefore, it is necessary to control the particle size and increase the surface area through the application of nanotechnology. The development of nanotechnology materials has attracted attention from various circles.[16] When used as an antibacterial material, nanoparticles have the advantage of a high ratio of surface area to volume and new properties.[9,17] This causes an increase in chemical activity and adsorption capacity against target contaminants which creates more significant potential in combating bacteria.[18]

One of the best materials for photocatalytic processes is titanium dioxide (TiO_2),[19] due to its several advantages such as high photocatalytic activity, good chemical stability, high oxidizing power, low toxicity, and ready availability.[19,20] Furthermore, it has been investigated as an antibacterial agent on *P. aeruginosa* to impair respiratory activity, destroy cells,[21] and increase polyunsaturated membrane phospholipids. Furthermore, the anatase phase of TiO_2 has energy corresponding to the reduction energy of O_2 in the photocatalytic process,[22] but its transformation to rutile limits the

[a]*Department of Chemistry, Padjadjaran University, Jln. Raya Bandung-Sumedang Km. 21, Indonesia. E-mail: diana.rahmawati@unpad.ac.id*

[b]*Graduate School of Science Education, University of Bengkulu, Jl. W. R Supratman, Bengkulu, Indonesia*

† Electronic supplementary information (ESI) available: Goodness of fit (GoF) equation and the Rietveld refinement plot for XRD analysis. See DOI: 10.1039/d1ra07043f

photocatalytic activity.[23] Also, TiO_2 has some drawbacks, such as agglomeration, which causes a reduction in surface area in solution.[24,25] However, this reduction is minimized by combining TiO_2 with other materials such as SiO_2,[23] ZnO,[26] Fe_2O_3,[27] and CuO.[28] Among the various types of supporting metal oxides, SiO_2 has various advantages because it minimizes recombination, increases adsorption capacity, and prevents agglomeration.[29] Erdural *et al.* (2014) added synthesized SiO_2 to TiO_2 photocatalyst with various concentrations, leading to inactivation ranging from 14.2 to 99.9% for *E. coli* bacteria.[30]

SiO_2 is obtained through synthesis or extraction from natural materials, both biological and non-biological.[23] To maximize natural resources, silica is obtained from the extraction of beach sand.[31] Based on data from the Ministry of Energy and Mineral Resources, Indonesian Geological Resources Center (2012), the total availability of silica sand is approximately 22.5 billion tons spread throughout Indonesia with 85% of the highest distribution on Sumatra Island, including Bengkulu Province.[32] Ishmah (2020) reported that 97.3% of silica had been successfully extracted from the beach in Bengkulu Province.[31] The incorporation of TiO_2 and silica increases photocatalytic activity by enlarging the surface area of the active sites of the photocatalyst and inhibiting the transformation from anatase to rutile.[20,33] Therefore, this study focuses on adding SiO_2 from beach sand extract to TiO_2 photocatalyst by a sonochemistry method and its application as an antibacterial against Gram-positive *Staphylococcus aureus* and Gram-negative *Pseudomonas aeruginosa*.

Results and discussion

Formation results of TiO_2 and TiO_2–SiO_2 nanocomposite

TiO_2–SiO_2 nanocomposite was synthesized with various mole ratios of 1 : 0.5; 1 : 1; and 1 : 2 using the sonochemistry method as shown in Fig. 1. Sonochemistry has been widely used to synthesize nano-sized materials.[34] To prepare the TiO_2–SiO_2 nanocomposite, titanium tetraisopropoxide (TTIP) was used as a precursor to form TiO_2. TTIP was reacted with isopropyl alcohol thereby causing the hydrolysis and condensation reactions to produce TiO_2.[35] The reaction mechanism for the formation of TiO_2 from TTIP is shown in Fig. 1.

This study used silica extracted from beach sand of Bengkulu, Indonesia based on a previous study.[31] The sonochemistry synthesis method was used with ultrasonic waves which cause smaller particles to form and increase size uniformity. The reaction products are obtained in the form of nanoamorphous and nanocrystalline particles.[34] These ultrasonic effects are summarized in reactions (1)–(7):[36]

$$H_2O \rightarrow H^{\bullet} + OH^{\bullet} \quad (1)$$

$$H^{\bullet} + H^{\bullet} \rightarrow H_2 \quad (2)$$

$$H^{\bullet} + OH^{\bullet} \rightarrow H_2O \quad (3)$$

$$OH^{\bullet} + OH^{\bullet} \rightarrow H_2O_2 \quad (4)$$

$$RH\ (\text{volatile vapor}) \rightarrow R^{\bullet} + H^{\bullet} \quad (5)$$

$$RH + OH^{\bullet}\ \text{or}\ H^{\bullet} \rightarrow R^{\bullet} + H_2O\ (\text{or}\ H_2) \quad (6)$$

$$Ti^{4+} + nR^{\bullet}\ (\text{or}\ H^{\bullet}) \rightarrow Ti^{0} \quad (7)$$

XRD characterization results

The diffractogram produced showed conformance to ICSD 98-015-6838 (ref. 37) for the anatase structure (tetragonal, space group $I4_1/amd$) and ICSD 98-016-5921 (ref. 38) for the rutile structure (tetragonal, space group $P4_2/mnm$). The synthesized TiO_2 crystals showed peaks at $2\theta = 25.2°$ (011), 37.8° (004), 47.8° (020), twin peaks at 53.9° (015) and 54.7° (121), 62.5 (024), twin peaks at 69.0° (116) and 70.1° (220), and 75.0° (125) as characteristic of TiO_2 anatase crystals. In the pattern of the TiO_2–SiO_2 nanocomposite, there are no additional peaks, but there is a change in the intensity and width of the peaks due to the addition of SiO_2. The results of XRD analysis of synthesized TiO_2, and TiO_2–SiO_2 nanocomposite with mole ratios 1 : 0.5; 1 : 1; and 1 : 2 are shown in Fig. 2.

Table 1 shows that the addition of SiO_2 affects the percentage of the crystal phase in the samples. TiO_2 and composites synthesized using the sonochemistry method had a high percentage of anatase (96.7–100.0%). These data demonstrate the role of ultrasonic waves in the formation of crystals in the

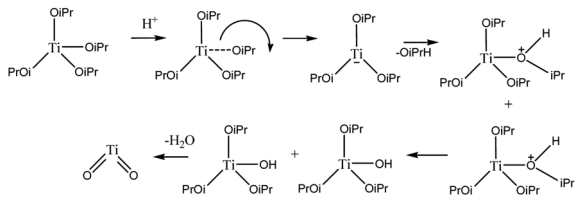

Fig. 1 Hydrolysis and condensation reactions to form TiO_2.

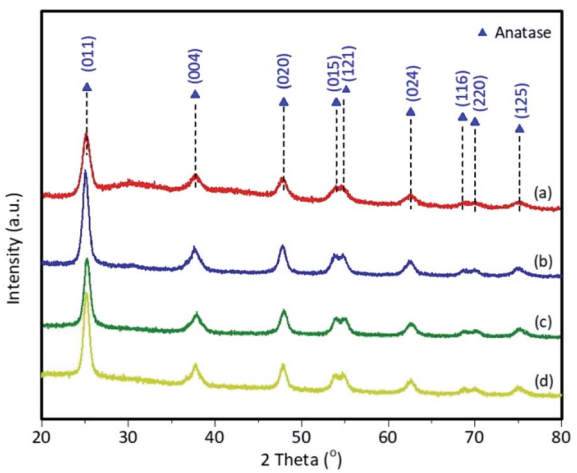

Fig. 2 XRD patterns for (a) synthesized TiO_2; (b) TiO_2–SiO_2 1 : 0.5; (c) TiO_2–SiO_2 1 : 1; (d) TiO_2–SiO_2 1 : 2.

Table 1 Phase percentages and Rietveld refinement parameters of the samples

	Phase (%)		Rietveld refinement parameters		
Sample	Anatase	Rutile	R_{exp}	R_{wp}	GoF
SiO_2	—	—	3.33	4.96	2.21
TiO_2	97.2	2.8	4.31	6.33	2.15
TiO_2–SiO_2 1 : 0.5	96.7	3.3	5.64	6.88	1.49
TiO_2–SiO_2 1 : 1	100.0	—	5.63	6.75	1.44
TiO_2–SiO_2 1 : 2	100.0	—	4.73	9.22	3.80

samples. Furthermore, the samples were prepared with a calcination temperature of 500 °C as the optimal temperature in the formation of TiO_2 with the anatase crystal structure.[39]

The XRD data showed that the addition of SiO_2 to the sample caused a reduction in the percentage of rutile structure in TiO_2. Similarly, TiO_2–SiO_2 1 : 1 and 1 : 2 composite samples did not have a rutile structure of TiO_2. Hence, the presence of SiO_2 inhibits the transformation from anatase to rutile. This is in accordance with Besançon *et al.* (2016).[20] Meanwhile, TiO_2 with anatase phase is the best for photocatalytic applications.[40] However, a small amount of rutile phase is still required in the photocatalysis process.

Habibi-Yangjeh *et al.* (2020) reported that a small amount of rutile phase in a TiO_2 photocatalyst is needed for electron transfer between crystalline phases, which functions to avoid recombination.[41]

To confirm the accuracy of the calculation from Rietveld refinement, the goodness of fit (GoF) value of the experimental XRD pattern with the XRD pattern calculated from the standard was calculated. The ideal value of GoF is 1.[42] In Table 1, it can be seen that the GoF value of the samples is in the range of 1.44–3.80. This value can still be categorized as good and acceptable (<4) because the XRD pattern obtained from the experimental results cannot be separated from noise so that the GoF value will be above 1. The Rietveld refinement plot is depicted in Fig. S1–S4.†

The crystallite size is calculated based on the Scherrer equation. The calculated crystallite size is the average of each phase peak in the XRD pattern and is calculated with the standard deviation. Table 2 shows that the addition of SiO_2 in a certain amount increases TiO_2 crystallinity. The TiO_2 sample had a crystallinity percentage of 64.4%; meanwhile, there was an increase in the crystallinity to 88.4% (TiO_2–SiO_2 1 : 0.5) when SiO_2 was added. However, this increase caused a decrease in the crystallinity percentage of the composite sample. This is because the amorphous structure of SiO_2 causes a reduction in crystallinity. High crystallinity is needed in photocatalysis to avoid the possibility of electron–hole recombination, thereby increasing photocatalytic activity.[43]

From the calculations using the Debye–Scherrer equation and Origin85 8.5.1 SR_2 software, the crystal size was obtained (Table 2). The crystal size in anatase and rutile was significantly different in the samples. Based on the data, the smallest anatase crystal size was obtained in the 1 : 1 composite. This indicates that the higher the silica concentration in the composite, the larger the crystallite size of anatase, while the rutile size tends to decrease. Fig. 3 shows the trend of crystal size and crystallinity of TiO_2 and the composites.

Therefore, based on the data obtained from XRD analysis, it was concluded that the addition of SiO_2 in a certain amount increases the crystallinity of TiO_2. Furthermore, SiO_2 plays a role in inhibiting the transformation from the anatase to the rutile phase.

Table 2 The crystal size of anatase and rutile (shown as the mean ± the standard deviation) and crystallinity percentages of the samples

	Crystal size (nm)		
Sample	Anatase	Rutile	Crystallinity (%)
SiO_2	—	—	11.90
TiO_2	8.36 ± 0.88	8.028 ± 0.82	64.48
TiO_2–SiO_2 1 : 0.5	9.09 ± 0.74	7.806 ± 0.97	88.39
TiO_2–SiO_2 1 : 1	9.91 ± 0.82	—	71.44
TiO_2–SiO_2 1 : 2	10.48 ± 0.74	—	56.07

FTIR characterization results

FTIR analysis was carried out to identify the functional groups in SiO_2, synthesized TiO_2, and TiO_2–SiO_2 composites in the wavenumber range of 400–1400 cm^{-1}. Fig. 4 shows the infrared spectra of the samples. In the TiO_2–SiO_2 nanocomposite spectra, there was signals of siloxane (Si–O–Si) and Ti–O–Ti, which proves that the sample contains both functional groups (Table 3), while Ti–O–Si bonds were evidenced at a wavenumber of 783–803 cm^{-1}.

Furthermore, the presence of a Ti–O–Si vibration peak indicates that the interaction between TiO_2 and SiO_2 is a chemical reaction (chemical bonding occurs), and not a simple physical mixing process. Peaks corresponding to Ti–O–Ti bonds appear at a wavenumber of 723–739 cm^{-1}. Based on FTIR data, the TiO_2–SiO_2 nanocomposite sample shows the presence of Ti–O–Ti, Si–O–Si, and Ti–O–Si, thereby indicating the presence of bonds from the two metal oxides.

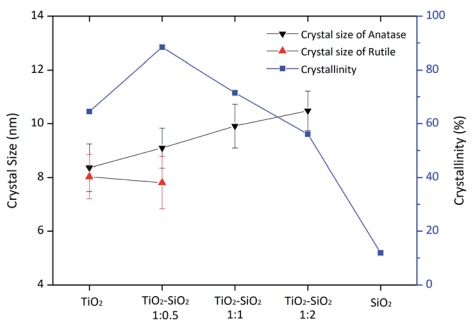

Fig. 3 Changes in crystal size of anatase and rutile, and variation of crystallinity of the composites.

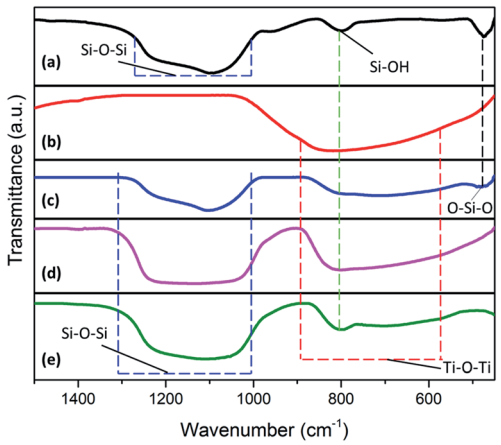

Fig. 4 Infrared spectra of (a) silica extract; (b) synthesized TiO_2; (c) TiO_2–SiO_2 1 : 0.5; (d) TiO_2–SiO_2 1 : 1; (e) TiO_2–SiO_2 1 : 2.

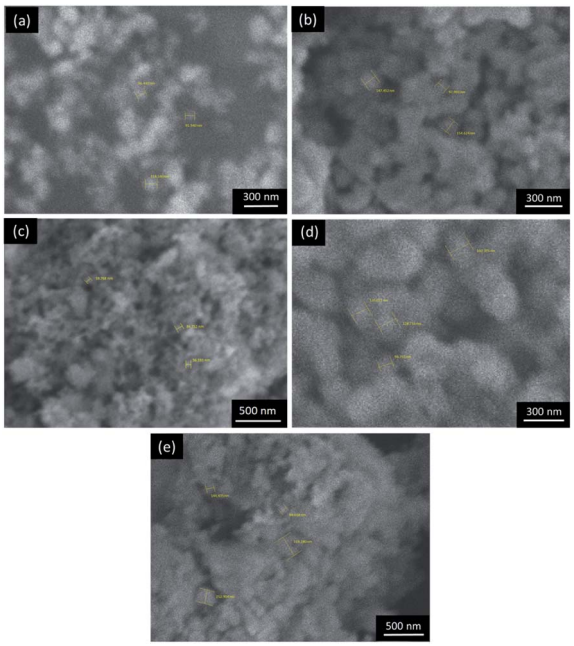

Fig. 5 SEM images of the samples to determine size distribution: (a) synthesized TiO_2, (b) SiO_2 extract, (c) TiO_2–SiO_2 1 : 0.5, (d) TiO_2–SiO_2 1 : 1, (e) TiO_2–SiO_2 1 : 2.

SEM-EDX characterization results

The morphology of the composite samples was studied using SEM, which showed inhomogeneous spherical particles (Fig. 5c–e). However, some particle agglomeration occurred in the various composite samples. In the synthesized TiO_2 (Fig. 5b) and the 1 : 2 TiO_2–SiO_2 composite (Fig. 5e), the agglomeration showed coalescence into quite large particles. Meanwhile, high agglomeration tends to reduce the active site of the photocatalyst. The results showed that the addition of SiO_2 reduces the agglomeration of TiO_2. Hence, a nanoparticle-sized sample is formed. This is also influenced by SiO_2, which complements the size of the TiO_2 photocatalyst. However, an extremely high addition of SiO_2 causes greater agglomeration due to the interaction between SiO_2; hence, it affects the surface area of the active sites in the catalyst.

Based on the SEM imaging results, the size distribution was determined using ImageJ 1.52a software from Fig. 5 (Wayne Rasband, National Institutes of Health).[45] The results showed that there was a significant reduction in particle size of the synthesized TiO_2 (Fig. 6b) and TiO_2–SiO_2 1 : 0.5 (Fig. 6d). These results indicate that SiO_2 reduces the aggregation of TiO_2. However, the addition of SiO_2 to the composite causes an increase in particle size due to agglomeration. Based on the results of the particle size distribution, the composite sample was categorized as nano-sized with a dominant size of less than 100 nm.

Furthermore, EDX qualitative analysis was carried out to determine the composition of the samples. This analysis is based on the X-ray radiation emitted from the atoms in a sample. Table 4 shows the EDX analysis results of extracted SiO_2, synthesized TiO_2, and TiO_2–SiO_2 composites with mole ratios of 1 : 0.5; 1 : 1; and 1 : 2. Based on the results, the percentage of Si atoms increases with the amount of silica being composited.

Photocatalytic antibacterial activity test results

The antibacterial activity of the samples was evaluated qualitatively and quantitatively using dilution and optical density methods, respectively. TiO_2–SiO_2 nanocomposite sample was tested for photocatalytic activity as an antibacterial agent against *Staphylococcus aureus* and *Pseudomonas aeruginosa* compared with the positive control (amoxicillin), negative control (without treatment), synthesized TiO_2, P25 Degussa (commercial TiO_2), and SiO_2 extract.

The photocatalytic test of *S. aureus* (Gram-positive bacterium) produced excellent results. Based on the antibacterial test using the optical density method, all nanocomposite samples showed antibacterial activity with an inactivation percentage ranging from 97.9 to 98.69% (Fig. 7). Furthermore, the

Table 3 Types of vibration in the samples based on the peaks that appear at each wavenumber[23]

Bond type	SiO_2	TiO_2	TiO_2 : SiO_2 (1 : 0,5)	TiO_2 : SiO_2 (1 : 1)	TiO_2 : SiO_2 (1 : 2)
Si–O–Si	1091 cm^{-1}	—	1103 cm^{-1}	1131 cm^{-1}	1111 cm^{-1}
Ti–O–Ti	—	667 cm^{-1}	723 cm^{-1}	751 cm^{-1}	739 cm^{-1}
Ti–O–Si	—	—	783 cm^{-1}	803 cm^{-1}	803 cm^{-1}
Si–OH	799 cm^{-1}	—	—	—	—
O–Si–O	475 cm^{-1}	—	467 cm^{-1}	—	—

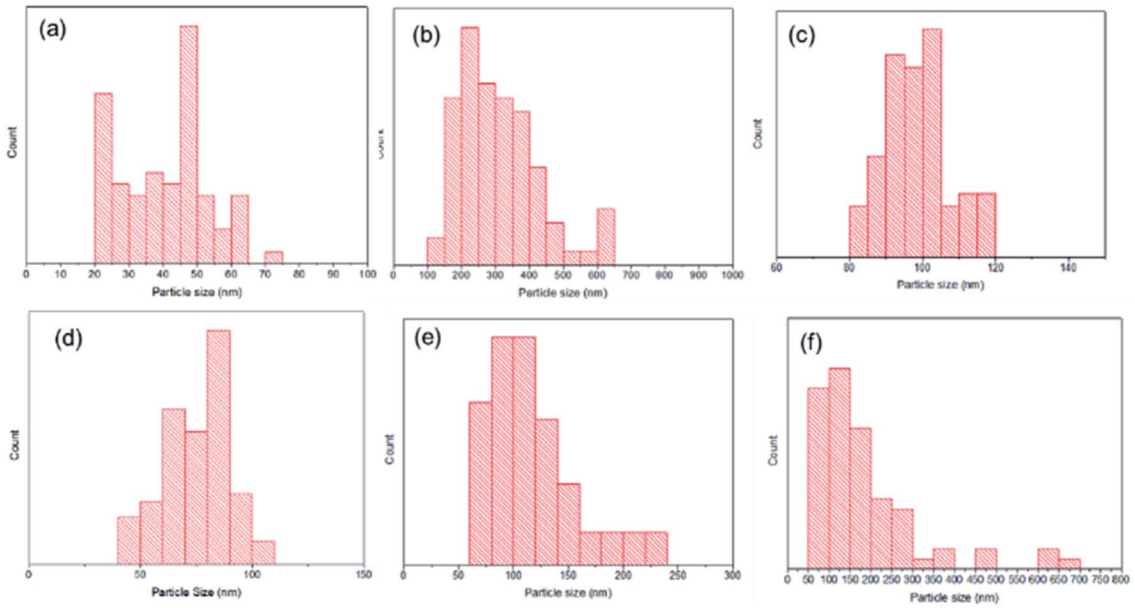

Fig. 6 Bar chart of sample particle size distribution: (a) TiO_2 P25 Degussa[44] (8–11 nm), (b) synthesized TiO_2 (108–637 nm), (c) SiO_2 extract (81–119 nm), (d) TiO_2–SiO_2 1 : 0.5 (40–107 nm), (e) TiO_2–SiO_2 1 : 1 (61–219 nm), (f) TiO_2–SiO_2 1 : 2 (73–698 nm).

antibacterial test using the dilution method showed perfect inhibition by the positive control and nanocomposite samples. The positive control (amoxicillin) belongs to the class of beta-lactam antimicrobials that bind to penicillin-binding proteins that inhibit transpeptidation, *i.e.*, the cross-linking process in cell wall synthesis, leading to the activation of autolytic enzymes in the bacterial cell wall.[46] P25 also showed bacterial inhibition, but certain bacteria were still growing. Meanwhile, the synthesized SiO_2 and TiO_2 showed low antibacterial activity.

Furthermore, the photocatalytic test on *P. aeruginosa* (Gram-negative bacterium) produced excellent results. Based on the antibacterial test using the optical density method, the nanocomposite samples had an inactivation percentage ranging from 88.95 to 97.44% (Fig. 8). Meanwhile, the antibacterial test using the dilution method showed complete inhibition by the positive control, TiO_2 P25 Degussa, as well as TiO_2–SiO_2 nanocomposites 1 : 0.5 and 1 : 1. TiO_2–SiO_2 nanocomposite 1 : 2 showed the presence of bacterial growth on the media, while TiO_2 P25 Degussa showed inhibition, but certain bacteria were still growing according to the dilution method (Fig. 8). P25 Degussa was used as a control for commercial TiO_2 nanoparticles which have been shown to have photocatalytic activity.[8] Although not significant, the 1 : 0.5 nanocomposite sample had a better level of bacterial activation compared to P25 Degussa. Moreover, the synthesized SiO_2 and TiO_2 extracts showed poor inhibition but still had antibacterial activity. Therefore, for both bacteria, the synthesized samples showed a relatively good inactivation percentage due to the dominant anatase structure which increases photocatalytic activity compared to previous studies.

Fig. 9 shows the difference in bacterial inactivation percentage with and without irradiation. These results indicate that the nanocomposite has significantly poor antibacterial activity in the no-irradiation condition. Meanwhile, SiO_2 still has antibacterial activity, given that it is not a photocatalyst material.[47]

In the antibacterial test, the best photocatalytic results were shown by the TiO_2–SiO_2 1 : 0.5 nanocomposite using optical density and dilution methods. This composite showed better results than separated TiO_2, indicating that the addition of SiO_2 increased the antibacterial activity of the sample. The role of the addition of SiO_2 is described in Scheme 1. The mechanism of SiO_2 as a photocatalyst supporting material has been described by Bahadur *et al.* (2019)[48] where the excited electrons move from

Table 4 Percentage of atoms in the sample from the EDX analysis

	Sample												
	TiO_2		SiO_2		TiO_2–SiO_2 1 : 0.5			TiO_2–SiO_2 1 : 1			TiO_2–SiO_2 1 : 2		
(%)	O	Ti	Si	O	Ti	O	Si	Ti	O	Si	Ti	O	Si
Weight	33.44	66.56	47.07	52.93	40.38	47.66	11.96	36.75	49.94	13.31	34.84	48.21	16.96
Atomic	60.07	39.93	33.62	66.38	19.84	70.13	10.03	17.59	71.55	10.86	16.75	69.36	13.89

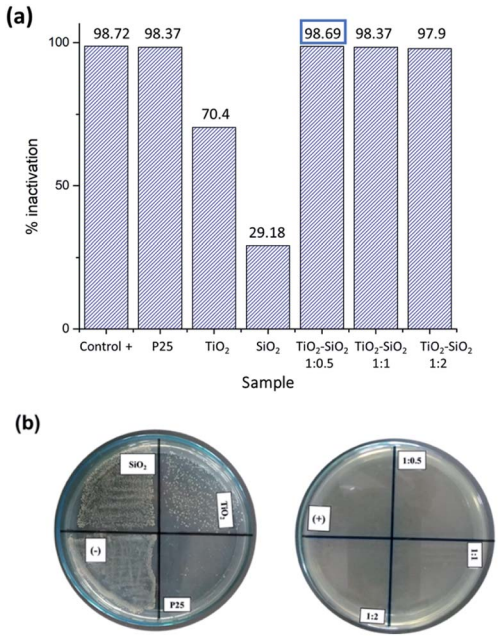

Fig. 7 Photocatalytic activity test results for *S. aureus* (Gram-positive bacterium): (a) optical density method, (b) dilution method.

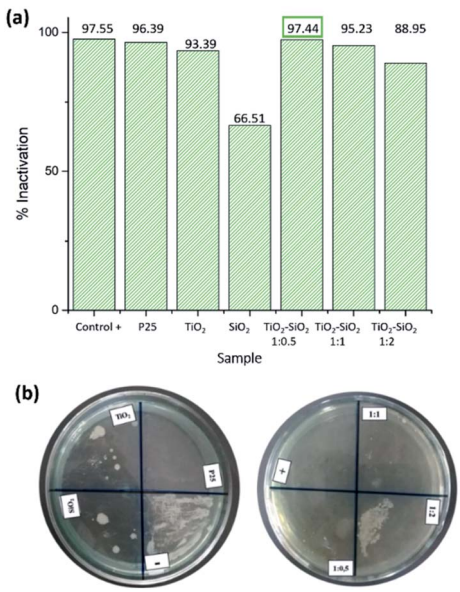

Fig. 8 Photocatalytic activity test results for *P. aeruginosa* (Gram-negative bacterium): (a) optical density method, (b) dilution method.

the TiO_2 surface to the SiO_2 surface as electron storage thereby increasing photo-generation for the photocatalyst process. The nanocomposite activity was influenced by the crystal phase, crystallinity, and particle size. These three aspects are presumably related to the ROS generated from the photocatalysis of the nanocomposite. The greater the amount of ROS produced, the better the photocatalytic activity in inactivating bacteria.[13,14] However, an extremely high addition of SiO_2 caused a decrease in activity due to agglomeration.

The test shows that SiO_2 has antibacterial activity because it is already of a nanoparticle size. Nano-SiO_2 interacts with living cells such as bacteria and interferes with cell functions such as cell differentiation, adhesion, and spread.[47]

Furthermore, the antimicrobial activity of SiO_2 was more significant at the nanoscale size due to the increased surface area.[49] However, SiO_2 showed poor antibacterial activity against *S. aureus*. The antibacterial activity in this study is in accordance with Erdural *et al.* (2014),[30] who used SiO_2 from synthetic chemicals; hence, this study shows that the use of SiO_2 from natural materials is effective in inactivating bacteria.

Experimental

Materials

The materials used consisted of distilled water, amoxicillin (Hexpharm), 70% ethanol (Sigma-Aldrich), *Staphylococcus aureus* (ATCC No. 35696), *Pseudomonas aeruginosa* (ATCC No. 27317), absolute ethanol (C_2H_5OH, 100%, Merck), silica extract from beach sand (Bengkulu, Indonesia), isopropyl alcohol (99%, Sigma-Aldrich), yeast nitrogen base media (MD 21152, Difco), titanium dioxide (TiO_2, P25 Degussa, Merck), and TTIP (97%, Sigma-Aldrich). All materials were used without prior treatment.

Synthesis of TiO_2 nanocomposite

The sonochemistry synthesis method was used according to Rosales *et al.* (2018),[50] while the synthesized TiO_2 was compared with the uncomposited samples. The synthesis was carried out by preparing TTIP and adding isopropyl alcohol dropwise. Furthermore, the titanium dioxide sol was sonicated and distilled water was added for 20 minutes. The solution was centrifuged at 6000 rpm, while the formed TiO_2 was dried for 2 hours and calcined at 500 °C for 5 hours.

Synthesis of TiO_2–SiO_2 nanocomposite

The synthesis method used was sonochemistry in line with Rosales *et al.* (2018).[50] The TiO_2–SiO_2 nanocomposite was synthesized by preparing TTIP and adding isopropyl alcohol dropwise; meanwhile, the silica used was extracted from beach sand based on Ishmah *et al.* (2019).[31] The extracted silica powder was ground with a PM 100 ball mill (Retsch), while the prepared solution consisting of distilled water and absolute ethyl alcohol was stirred sonochemically in a 900 W sonicator (BEM-900A, Bueno Biotech). Furthermore, this solution was mixed with silica and also stirred, while the titanium and silicon dioxide sols were also mixed in the sonicator. Subsequently, distilled water was added and stirred continuously in a sonicator for 20 minutes. The solution was centrifuged at 6000 rpm, while the formed TiO_2–SiO_2 nanocomposite was dried and calcined at 500 °C for 5 hours. This procedure was carried out for TiO_2–SiO_2 nanocomposite with various mole ratios of 1 : 0.5, 1 : 1, and 1 : 2.

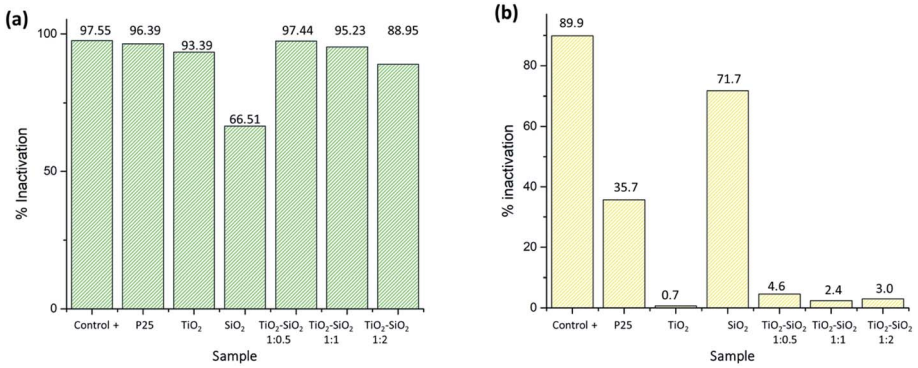

Fig. 9 Bacterial inactivation percentage against *Pseudomonas aeruginosa* (a) with and (b) without irradiation.

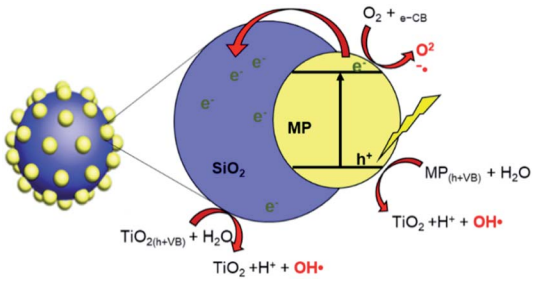

Scheme 1 The role of SiO_2 in TiO_2 photocatalyst performance.[48]

Sample characterization

X-ray diffraction (XRD) analysis was performed to identify the extracted silica crystal lattice and the synthesized TiO_2–SiO_2 nanocomposite. Both components were analyzed by XRD (Rigaku/MiniFlex 600), with measurements carried out at room temperature using Cu Kα radiation at an angle of 2θ from 20° to 80°. Furthermore, the crystal structure was refined using the Rietveld method with HighScore Plus software (PANalytical 3.0.5), while the crystal size was determined using the Debye–Scherrer eqn (8):

$$D = \frac{K\,\lambda}{B\cos\theta} \tag{8}$$

with D being the crystal size, K the Scherrer constant (0.89), λ the wavelength of X-ray radiation (0.154 nm), B the value of FWHM (full width at half maximum) of the peak (radians), and θ the angle of diffraction (radians). The crystallinity of the sample is calculated using Origin85 8.5.1 SR2 software to be able to calculate the area of the crystalline phase as well as the area of the amorphous phase. Percent crystallinity is determined by eqn (9):

$$\text{crystallinity}(\%) = \frac{\text{crystal phase area}}{\text{crystal phase area} + \text{amorphous phase area}} \times 100\% \tag{9}$$

Then, SEM-EDS (scanning electron microscopy-energy dispersive X-ray spectrometry) analysis was conducted with a Hitachi SU 3500 using 5 kV at a magnification of 10 000×. Analysis was performed to determine the morphological shape of the surface and composition of the sample. Photocatalysts of TiO_2–SiO_2 nanocomposite were further characterized using FTIR (Fourier-transform infrared spectroscopy), with a PerkinElmer Spectrum 100 (Massachusetts, USA) to determine the functional groups of silica extract as well as TiO_2–SiO_2 nanocomposites. FTIR was used with a scanning range of 400–1400 cm^{-1}. This analysis is done by mixing samples that had been finely eroded with dry KBr powder. This mixing was done in agate.

Antibacterial activity test

(a) Dilution method. Antibacterial testing in this study was done using the modified dilution method.[51] The bacteria *Staphylococcus aureus* and *Pseudomonas aeruginosa* were taken using a micropipet into sterile test tubes that contained samples. Sample types include positive control (amoxicillin), negative control (no treatment), synthesized TiO_2, P25 Degussa (commercial TiO_2), SiO_2 extract, and various TiO_2–SiO_2 nanocomposites (1 : 0.5; 1 : 1; 1 : 2). The sample was illuminated with a mercury lamp (HPL-N 125 W Philips) at a distance of 30 cm for 2 hours with stirring. A Petri dish containing media was divided into 4 quadrants. Next, the sample was flattened on a medium surface to each quadrant on the Petri dish. The sample was incubated for 12 hours.

(b) Optical density method. The optical density method was performed to determine the inactivation of bacteria quantitatively. This method refers to the modified Khashan *et al.* (2016) research method.[52] The bacteria *Staphylococcus aureus* and *Pseudomonas aeruginosa* were taken using a micro-pipet of 1 mL into a sterile test tube that contained 30 mg of the sample. Sample types include positive control (amoxicillin), negative control (without treatment), synthesized TiO_2, P25 Degussa (commercial TiO_2), SiO_2 extract, and various TiO_2–SiO_2 nanocomposites (1 : 0.5; 1 : 1; 1 : 2). The sample was illuminated with a mercury lamp (HPL-N 125 W Philips) at a distance of 30 cm for 2 hours with stirring. The sample was incubated for 12 hours. Then, the absorbance value of the sample was measured at a wavelength of 600 nm using a UV-visible spectrophotometer. The percentage of bacterial inactivation is calculated by

comparing the absorbance of the sample with the absorbance of the negative control, represented by eqn (10):

$$\%\ \text{inactivation} = \frac{\text{OD}_{\text{control negative}} - \text{OD}_{\text{sample}}}{\text{OD}_{\text{control negative}}} \times 100\% \quad (10)$$

Conclusions

The antibacterial activity test against Gram-positive *Staphylococcus aureus* and Gram-negative *Pseudomonas aeruginosa* shows that TiO_2–SiO_2 nanocomposite has a better inactivation activity than TiO_2. The addition of natural silica to the TiO_2 photocatalyst affects the crystallinity percentage, crystal size, and particle size. Furthermore, there was an increase in the crystallinity percentage of TiO_2–SiO_2 nanocomposites. TiO_2–SiO_2 nanocomposite with a ratio of 1 : 0.5 shows the best antibacterial activity with inactivation percentages of *S. aureus* and *P. aeruginosa* of 98.60% and 97.44%, respectively. Based on the results, the addition of SiO_2 increases the photocatalytic activity of TiO_2 as an antibacterial agent. The results of this study provide an alternative antibacterial agent produced by using environmentally friendly natural materials.

Author contributions

Conceptualization, D. R. E. and M. L. F.; methodology, A. L.; software, M. D. P. and A. L.; validation, D. R. E., M. L. F. and I. R.; formal analysis, A. L.; investigation, A. L.; resources, A. L.; data curation, A. L.; writing original draft preparation, A. L.; writing review and editing, Y. D., D. R. E., M. L. F. and M. D. P.; visualization, M. D. P.; supervision, D. R. E., Y. D. and M. L. F.; project administration, D. R. E.; funding acquisition, D. R. E. and I. R. All authors have read and agreed to the published version of the manuscript.

Conflicts of interest

There are no conflicts to declare.

Acknowledgements

Authors are grateful for the facilities from Universitas Padjadjaran, Indonesia by Academic Leadership Grant (ALG) Prof. Iman Rahayu (ID: 1959/UN6.3.1/PT.00/2021), Indonesian Ministry of Research by Penelitian Dasar Unggulan Perguruan Tinggi (PDUPT ID: 1207/UN6.3.1/PT.00/2021), and World Class Professor (WCP) 2021 grant.

References

1 M. Vouga and P. Greub, *Clin. Microbiol. Infect.*, 2015, **22**(1), 12–21.
2 K. W. Post, *Overview of Bacteria*, 2019.
3 Y. Li, J. H. Zhang, S. P. Hu, L. Wang and J. Q. Xin, *J. Mol. Catal. A: Chem.*, 2007, **261**, 131–138.
4 R. T. Sadikot, T. S. Blackwell, J. W. Christman and A. S. Prince, *Am. J. Respir. Crit. Care Med.*, 2005, **171**, 1209–1223.
5 M. Karambin and M. Zarkesh, *Iran. J. Pediatr.*, 2011, **21**, 83.
6 D. Cheng, H. Sun, J. Xu and S. Gao, *Vet. Microbiol.*, 2006, **115**, 320–328.
7 S. J. Thiele-Bruhn, *J. Plant Nutr. Soil Sci.*, 2003, **166**, 145–167.
8 Y. N. Slavin, J. Asnis, U. O. Häfeli and H. Bach, *J. Nanobiotechnol.*, 2017, **15**, 1–20.
9 M. J. Hajipour, K. M. Fromm, A. A. Akbar, d. A. Jimenez, D. Larramendi, I. R. de, T. Rojo, V. Serpooshan, W. J. Parak and M. Mahmoudi, *Trends Biotechnol.*, 2012, **30**, 499–511.
10 Y. Bena, C. Fua, M. Hua, L. Liua, M. H. Wong and C. Zheng, *Enviromental Res.*, 2019, **169**, 483–493.
11 Effendy, *Logam, Aloi, Semikonduktor, dan Superkonduktor*, Bayumedia Publishing, 2010.
12 M. B. Ahmed, J. L. Zhou, H. H. Ngo, W. Guo, N. S. Thomaidis and J. Xu, *Hazard. Mater.*, 2017, **323**, 274–298.
13 S. L. Percival, P. G. Bowler and D. J. Russell, *Hosp. Infect.*, 2005, **60**, 1–7.
14 K. H. Cho, J. E. Park, T. Osaka and S. G. Park, *Electrochim. Acta*, 2005, **51**, 956–960.
15 M. S. Nasrollahzadeh, M. Hadavifar and S. S. Ghasemi, *Appl. Water Sci.*, 2018, **8**, 104.
16 I. Khan, K. Saeed and I. Khan, *Arabian J. Chem.*, 2019, **12**, 908–931.
17 Y. Xia, *Nat. Mater.*, 2008, **7**, 758–760.
18 P. I. Dolez, *Nanomaterials Definitions, Classifications, and Applications*. Nanoengineering: Global Approaches to Health and Safety Issues, 2015.
19 S. Leong, A. Razmjou, K. Wang, K. Hapgood, X. Zhang and H. J. Wang, *J. Membr. Sci.*, 2014, **472**, 167–184.
20 M. Besançon, L. Michelin, L. Josien, L. Vidal, K. Assaker, M. Bonne, B. Lebeau and J. L. Blin, *New J. Chem.*, 2016, **40**, 4386–4397.
21 Y. H. Tsuang, S. Jui-Sheng, H. Yu-Chen, L. Chung-Hsin, H. C. Walter and W. Chien-Che, *Artif. Organs*, 2008, **32**, 167–174.
22 R. Sellapan, *Mechanisms of Enhanced Activity of Model TiO_2/Carbon and TiO_2/Metal Nanocomposite Photocatalysts*, Chalmers University, 2013.
23 D. R. Eddy, S. N. Ishmah, M. D. Permana, M. L. Firdaus, 2020.
24 L. Wu, H. Yan, J. Xiao, X. Li and X. Wang, *Ceram. Int.*, 2017, **43**, 9377–9381.
25 L. Pinho and M. J. Mosquera, *Appl. Catal., B*, 2013, **134–135**, 205–221.
26 J. Tian, L. Chen, Y. Yin, X. Wang, J. Dai, Z. Zhu, X. Liu and P. Wu, *Surf. Coat. Technol.*, 2009, **204**, 205–214.
27 N. Davari, M. Farhadian, A. R. S. Nazar and M. J. Homayoonfal, *J. Environ. Chem. Eng.*, 2017, **5**, 5707–5720.
28 H. Koohestani and S. K. Sadrnezhaad, *Water Treat*, 2016, **57**, 22029–22038.
29 H. Ijadpanah-Saravi, M. Zolfaghari, A. Khodadadi and P. Drogui, *Desalin. Water Treat.*, 2016, **57**, 14647–14655.

30 B. Erdural, U. Bolukbasi and G. J. Karakas, *J. Photochem. Photobiol., A*, 2014, **283**, 29–37.
31 S. N. Ishmah, M. D. Permana, M. L. Firdaus and D. R. Eddy, *J. Sci. Educ. Technol.*, 2020, **4**, 1–5.
32 Kementrian Energi dan Sumber Daya Mineral Pusat Sumber Daya Geologi, Neraca Sumber Daya Mineral Non Logam di Indonesia, *Laporan Tahunan Badan Geologi*, ed. E. B. Lelono, 2012.
33 M. Yaseen, Z. Shah, R. C. Veses, S. L. P. Dias, E. C. Lima, R. Sdos Glaydson, J. C. P. Vaghetti, W. S. D. Alencar and K. J. Mehmood, *J. Anal. Bioanal. Tech.*, 2017, **08**, 8–11.
34 C. Y. Teh, T. Y. Wu and J. C. Juan, *Chem. Eng. J.*, 2017, **317**, 586–612.
35 P. Chaudhari, V. Chaudhari and S. Mishra, *Indonesian geological agency annual report*, 2016, 19, pp. 446–450.
36 H. Xu, B. W. Zeiger and K. S. Suslick, *Chem. Soc. Rev.*, 2013, **42**, 2555–2567.
37 F. Liu, S. H. Garofalini, D. King-Smith and D. Vanderbilt, *Phys. Rev. B*, 1994, **49**, 12528.
38 Z. B. M. G. Jian, *Chin. J. High Pressure Phys.*, 2006, **20**, 211–216.
39 S. Murugesan, P. Kuppusami and E. Mohandas, *Mater. Res. Bull.*, 2010, **45**, 6–9.
40 W. Zhang, A. Weidenkaff and R. Armin, *Mater. Lett.*, 2001, 3429.
41 H. A. Kiwaan, T. M. Atwee, E. A. Azab and A. A. J. El-bindary, *Mol. Struct.*, 2020, **1200**, 127115.
42 B. H. Toby, *Powder Diffr.*, 2006, **21**, 67–70.
43 A. Habibi-Yangjeh, S. Asadzadeh-Khaneghah, S. Feizpoor and A. J. Rouhi, *Colloids Interface Sci.*, 2020, **580**, 503–514.
44 H. Zheng, H. Svengren, Z. Huang, Z. Yang, X. Zou and M. Johnsson, *J. Phys. Chem. Solids*, 2019, **130**, 180–188.
45 I. Kustiningsih, S. Slamet and W. W. Purwanto, *Reaktor*, 2015, **15**, 205–212.
46 M. D. Abràmoff, P. J. Magalhães and S. J. Ram, *Biophotonics Int.*, 2004, **11**, 36–42.
47 D. J. Weber, N. E. Tolkoff-Rubin and R. H. Rubin, *Pharmacotherapy*, 1984, **4**, 122–136.
48 S. M. Dizaj, F. Lotfipour, M. Barzegar-Jalali, M. H. Zarrintan and K. Adibkia, *Mater. Sci. Eng., C*, 2014, **44**, 278–284.
49 N. M. Bahadur, F. Chowdhury, M. Obaidullah, M. S. Hossain, R. Rashid, Y. Akter, T. Furusawa, M. Sato and N. J. Suzuki, *Nanomater*, 2019, 1–11.
50 V. Dhapte, S. Kadam, V. Pokharkar, P. K. Khanna and V. Dhapte, *ISRN Inorg. Chem.*, 2014, 1–8.
51 A. Rosales, A. Maury-Ramírez, R. M. Gutiérrez, D. C. Guzmán and K. Esquivel, *Coatings*, 2018, **8**, 1–13.
52 K. S. Khashan, G. M. Sulaiman and F. A. Abdulameer, *Arabian J. Sci. Eng.*, 2016, **41**, 301–310.